Atomic force microscopy of bacteria reveals the mechanobiology of pore forming peptide action

Anna Mularski[1], Jonathan J. Wilksch[2], Eric Hanssen[3], Richard A. Strugnell[2], Frances Separovic[1]*

[1] School of Chemistry, The University of Melbourne, VIC 3010 Australia

[2] Department of Microbiology and Immunology, The Peter Doherty Institute for Infection and Immunity, The University of Melbourne, VIC 3010, Australia

[3]Advanced Microscopy Unit, Bio21 Molecular Science and Biotechnology Institute, The University of Melbourne, VIC 3010, Australia

*Corresponding author

Keywords: atomic force microscopy, *Klebsiella pneumoniae*, antimicrobial peptide, capsular polysaccharide, membrane interaction, caerin, melittin

Abstract

Time-resolved AFM images revealed that the antimicrobial peptide (AMP) caerin 1.1 caused localised defects in the cell walls of lysed *Klebsiella pneumoniae* cells, corroborating a pore-forming mechanism of action. The defects continued to grow during the AFM experiment, becoming large holes that were also visualised by scanning electron microscopy. Evidence of damaged cytoplasmic membranes was visualised by cryo-EM using the same peptide concentration as in the AFM experiments. At three times the minimum inhibitory concentration of caerin, 'pores' were visible in the outer membrane. The capsule of *K. pneumoniae* AJ218 was unchanged by exposure to caerin, indicating that the ionic interaction of the positively charged peptide with the negatively charged capsular polysaccharide is not a critical component of AMP interaction with *K. pneumoniae* AJ218 cells. Further, the presence of a capsule confers no advantage to wild-type over capsule-deficient cells when exposed to the AMP caerin.

Introduction

Throughout the plant and animal kingdoms, antimicrobial peptides (AMPs) are part of the host organism's innate defence response.[1] AMPs show promise as an alternative to conventional antibiotics: [2, 3] their minimum inhibitory concentrations (MICs) are in the low micromolar range, and comparable to the active concentrations of commercially available antibiotics against sensitive organisms. [4] The activity of most AMPs has been attributed to membrane disruption, either via a detergent-like or pore-forming mechanism, [5] although studies have proposed mechanisms in which, following membrane permeabilisation, AMPs target intracellular cell components as the killing mechanism. [3, 6] In either case, the

mechanism of AMP-induced membrane permeabilisation remains unclear, and warrants further investigation. Phospholipid membranes have been used extensively to study the mode of action of AMPs. These model systems lack the complexity of the bacterial surface and cell wall, but have demonstrated that phospholipid charge [7, 8] and membrane curvature [9-11] influence the mode of interaction. The size, structure and hydrophobicity of the peptide also affect its selectivity and activity. [12] However, studies of the interactions of AMPs with model membrane systems and live bacteria often yield contradictory results, [13-17] which emphasise the importance of *in situ* studies.

Caerin 1.1 (GLLSVLGSVAKHVLPHVVPVIAEHL-NH_2) is a major component of the skin gland secretions of the Australian tree frogs of the genus *Litoria*. [18] Like many AMPs, caerin 1.1 is an unstructured random coil in solution, rearranging into an amphipathic α-helix on partitioning into membrane or membrane mimetic environments. [11] It has wide spectrum antibiotic activity [19] although the peptide is more specific to Gram-positive bacteria. This has been attributed to more complex protective structures separating the inner workings of Gram-negative bacterial cells from their environments. [11] Caerin has also shown anticancer [20] and antiviral [21] activity and has been characterised by quartz crystal microbalance [22], surface plasmon resonance [23], circular dichroism and nuclear magnetic resonance [16] studies.

Atomic force microscopy (AFM) is a proven technique for the study of biological samples *in situ* [24, 25]. The physical properties of living biological cells can be studied under physiologically relevant conditions that require little sample preparation and without destruction of the sample. [26-29] Properties such as cytoplasmic turgor pressure, cell wall elasticity and long-range electrostatic interaction can be determined using AFM [30, 31]. Of

particular relevance to this work are studies that have investigated how AMPs affect cell stiffness and adhesion in live bacteria. [15, 32-35] Here, we present AFM data that gives insight into the physiological responses of *Klebsiella pneumoniae* when exposed to the AMP, caerin 1.1.

K. pneumoniae is a source of shared antimicrobial resistance such as carbapenem-resistance and the extended-spectrum beta lactamases (ESBLs) [36, 37] and is also recognized as a serious cause of hospital-acquired infections. A loosely organised polysaccharide layer (known as the capsule) is assembled around the *K. pneumoniae* cell envelope. It takes the form of a hydrated polyelectrolyte network and can grow up to several hundred nanometers thick. [38] The capsule provides protection from environmental stresses, such as antibiotics, detergents, desiccation and the host's immune response. [39] The exopolysaccharide capsule also plays a role in the formation of biofilms on surfaces. [40] Further, a direct association has been discovered between capsular size and pathogenicity of isolates in animal models. [41] Since AMPs must first pass through this network, the role of the capsule in the mode of action of caerin warrants investigation.

The resistance of a capsule-deficient *K. pneumoniae* mutant to the AMPs, α-defensin-1 and polymyxin B, was increased following the addition of purified capsular polysaccharides. [42] The negatively charged bacterial capsule was proposed to act as an effective decoy, enabling encapsulated cells to resist cationic AMPs. The AMPs were postulated to trigger the release of capsular material *in vivo,* which in turn protect bacteria against AMPs. Previously [35], we used AFM capsule thickness measurements to demonstrate that the entropic drive of the peptide to associate with the bacterial membrane dominates over long-range electrostatic attraction between a cationic peptide and the negatively-charged *K. pneumoniae* capsule. The

long-range electrostatic attraction, however, may first attract the peptides to bacterial cells. These results do not negate the idea that extracellular capsular polysaccharides play a role in protecting bacterial cells from AMPs.

The melittin-derived peptide used previously (GIGAVLKVLTTGL**K**ALISWIKRKRQQ-NH_2) is structurally very similar to caerin 1.1, and is one more amino acid in length. Caerin [43] is one of several closely related peptides that appear to act by fundamentally different mechanisms depending on their length. In the same model membranes, the shorter of these peptides, aurein and citropin, have been shown to act via a detergent-like mechanism whereas the longer peptides, caerin and -maculatin, use a pore-forming mechanism.

In this work we present time-resolved AFM images that revealed caerin caused local defects in the cell wall of lysed *K. pneumoniae*, which supports a pore-forming mechanism of action. These defects continued to grow, becoming large holes that also were visualised using scanning electron microscopy. Further, we present data which demonstrate that the *K. pneumoniae* AJ218 capsule did not confer an advantage over capsule-deficient *K. pneumoniae* AJ218. The *K. pneumoniae* AJ218 capsule appeared to be unaffected by peptide exposure which indicates that ionic interaction of peptide and bacteria-bound capsular polysaccharide is not a critical component of *K. pneumoniae* AJ218 interaction with caerin.

Experimental

1. Peptides

Caerin 1.1 was purchased from Bio21 Peptide Technology, University of Melbourne.

Melittin was purchased from Mimotopes (Clayton, Australia). Peptides were synthesized by solid-phase techniques and were >95% pure.

2. Bacterial strains, culture conditions, and harvesting

Klebsiella pneumoniae AJ218 (capsule serotype K54) is a human urinary tract infection isolate, identified at the microbiological laboratory of the Alfred Hospital, Melbourne, Australia. [44, 45] All strains were maintained on Luria-Bertani (LB) agar at 37°C. LB broths inoculated with these cultures were grown for 16 hours at 37°C while shaking (180 rpm). Stationary phase cells were then harvested by centrifugation (10 min at 3500 × g) and washed twice with Milli-Q™ water (18.2 MΩ cm^{-1}). The final concentration of bacterial cells in Milli-Q™ water was approximately 2×10^8 CFU mL^{-1}.

A *wzc* mutant of *K. pneumoniae* AJ218, defective in the transporter that enables capsule polysaccharide export, was isolated following random mini-Tn*5Km2* transposon insertion mutagenesis [46] of *K. pneumoniae* AJ218. To confirm transposon insertion within the *wzc* gene, Y-linker ligation PCR and subsequent DNA sequencing analysis of the transposon-flanking region was performed to ensure correct location of the mutation. [47]

The minimum inhibitory concentration (MIC) and minimum bactericidal concentration (MBC) of caerin was determined for both wild-type and capsule-deficient *K. pneumoniae* cells using the microdilution broth method outlined by the National Committee for Clinical Laboratory standards. [48]

3. Viable count assay

Cell suspensions of *K. pneumoniae* AJ218 wild-type and capsule-deficient strains were incubated in 10 mM HEPES buffer (pH 7.4) at 37°C in the presence or absence of 6 μM peptide solution. At hourly time-points, aliquots were removed from suspensions and then diluted on agar media to determine the viable number of bacteria (expressed as colony forming units per mL, cfu/mL).

4. Bacterial sample conditions for AFM measurements

Gelatine-coated glass slides were used to immobilize bacteria for AFM measurements. In previous work [30, 35] PEI-coated slides were used for wild-type cells. The PEI and gelatine coating methods are described [30] When treated with caerin 1.1, *K. pneumoniae* AJ218 did not adhere firmly enough to PEI-coated slides for force measurements. Substrate rigidity is a requirement when measuring cell indentation to ensure that only cell compression contributes to the measurement. Wang *et al*. [30] have shown that, even though gelatine may be expected to be a softer substrate than PEI, there is no measureable effect of gelatine deformability on the force profiles of the bacteria, which suggests that this method results in a gelatine layer sufficiently thin to present as a rigid surface in AFM force measurements.

All mechanical measurements were performed within 2-3 hours of removal of the bacteria from growth media. Bacteria-coated slides were immersed in 10 mM HEPES buffer (pH 7.4) or 6 μM peptide solution (made in 10 mM HEPES buffer, pH 7.4) and kept at rest within the calibrated AFM for at least 40 minutes before measurements commenced. Previous work has demonstrated that cells remain viable for the duration of the experiment as determined by live/dead cell fluorescence assays using a Molecular Probes Bacterial Viability Kit. [30]

An imaging volume of 5 mL was used. Measurements were conducted first in HEPES buffer and then exchanged for 1.2 μM peptide in HEPES buffer. To establish the lipid to peptide ratio at which experiments were conducted, bacteria attached to the slides were stained with crystal violet following AFM measurements, and viewed at 60x magnification. Counting cells in several areas of known size allowed for an approximation of the number of cells per slide. Ingraham *et al*. [49] give an approximation of the number of lipids per microbial cell, which allowed us to calculate the number of lipid molecules per slide. The lipid to peptide ratio for all experiments reported here, assuming all peptide is bound, was estimated to be 1:1. This is considerably higher than generally used with model membrane systems to ensure measurable peptide-cell interaction within the timeframe of the experiment.

5. Atomic force microscopy and force measurements

AFM measurements were performed using an MFP-3D instrument (Asylum Research, Santa Barbara, CA). Silicon nitride cantilevers were purchased from Bruker (MLCT, Camarillo, CA) with a nominal spring constant of 0.01 Nm^{-1} and probe radius of 20 nm (according to the manufacturer's specifications). Cantilever spring constants were determined using the thermal tune method [50] included in the MFP-3D software. Calibrated spring constants were within the range of 0.016-0.020 Nm^{-1}. All cantilevers used were from the same batch. All tips were cleaned in a BioForce UV/ozone cleaner (BioForce Nanosciences Inc, Ames, IA) before use. Photodetector sensitivity was measured on a clean silica slide prior to force measurements. [51] The slope of the constant compliance region of the force curves obtained was used to convert the deflection, d, in mV to nm. The cantilever defection was then converted into a force, F, according to Hooke's law, $F = k \times d$, where k is the force constant of the cantilever. [52]

Cells were imaged in contact mode at a scan rate of 1 Hz. Trace and retrace were monitored to locate the true apex of cells and ten force curves were measured at different locations along it. The cell apex was probed during force measurements rather than the cell periphery, which has a high degree of curvature that makes quantifying mechanical properties difficult. [53] Imaging was repeated after each collection of ten force curves to ensure no change in cell morphology had occurred. Force curves were acquired at a loading rate of 600 nm s^{-1}.

Force data at time zero (i.e., before the addition of peptide) were acquired by measuring 10 force curves per cell across a population of cells. The values obtained were averaged to provide a negative control and are in good agreement with prior reports [30, 35] under similar conditions. The force profiles acquired following the addition of peptide were measured on single wild-type cells over a ~2 hour time frame. At each time point, 10 force curves were measured and the median curve was selected for analysis. Ten single cell experiments were performed to ensure reproducibility in the observed trends over time. The error bars around each data point in the figures represent ±1 standard deviation, which was calculated for a set of 10 force curves in both buffer and 6 μM caerin solution. The data obtained showed good reproducibility from location to location along each cell apex and from cell to cell at comparable times of exposure to peptide (Supporting Information, Figure S1).

6. Bacterial cell indentation and force curve analysis

Force curves obtained from both cells for this work were analysed using Hooke's law:

$$F_{loading} = K_{bacterium}\delta \qquad (1)$$

where $F_{loading}$ is the applied loading force, $K_{bacterium}$ is the bacterial spring constant, and δ is the indentation. The slope of this linear compliance region of the force profile yields $K_{bacterium}$, which is a direct measure of the relative turgor pressure of the bacterium. [31, 52]

The indentation depth at which the linear portion of the force curve begins provides an estimate of the bacterial capsule thickness.

7. Cryo-electron microscopy

Bacteria were exposed to buffer or caerin solution for two hours before being absorbed on glow discharge holey carbon grids and plunge frozen in liquid ethane. The resulting grids were observed on a FEI Tecnai F30 operating at 300 kV under low dose. Each micrograph was recorded on a Gatan Ultrascan 1000 with a total dose of ~2,000 e/nm^2.

8. Scanning electron microscopy

Cells were adhered to coverslip surface with poly-L-lysine and then fixed in 2.5% gluteraldehyde. Cells were then dehydrated by rinsing with ethanol/water of increasing ethanol percentage. Coverslips were dried before sputter coating with a Dynavac sputter coater. Cells were visualised using a FEI Quanta FEG 200 ESEM at a voltage of 10.0 kV.

Results and Discussion

Following adhesion to PEI slides, bacterial cells were imaged in contact mode in HEPES buffer (10 mM, pH 7.4) both before and after each set of force measurements to ensure cells were well adhered to the surface. Figure 1a shows a typical 12 x 12 μm AFM image of well-dispersed, rod-shaped *K. pneumoniae* cells. The surfaces of the cells appeared topographically homogenous on this and smaller scale images (Figure 1b).

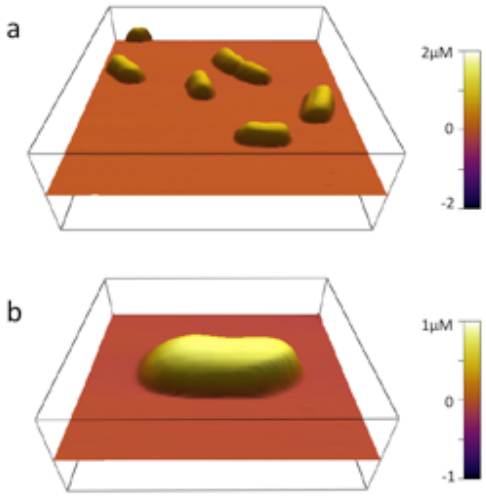

Figure 1. 3D projections of AFM images: (a) 12 × 12 µm image of topographically homogenous, rod shaped *K. pneumoniae* cells; and (b) 3 × 3 µm image of a single *K. pneumoniae* cell. All cells were imaged *in situ* (10 mM HEPES buffer, pH 7.4).

To provide statistically robust data in this study, force profiles of bacterial cell indentation were obtained at 10 points along the apex of each bacterium. Before measurements commenced, the system was allowed to equilibrate to minimise lateral drift. Images of cells before and after each set of force measurements were compared to confirm minimal drift. Highly reproducible force curves were collected in this way. (Supporting Information, Figure S1). In all experiments, maximum loading force was controlled to prevent bacterial cell wall rupture due to force measurements. [54] The contact point, i.e., zero indentation, is defined as the point at which contact was first made between the tip and the sample, correlates to the onset of cantilever deflection. Long-range non-contact double layer interactions are negligible in this study since the electrolyte concentration is 10 mM (corresponding to a Debye length of ~ 3nm).

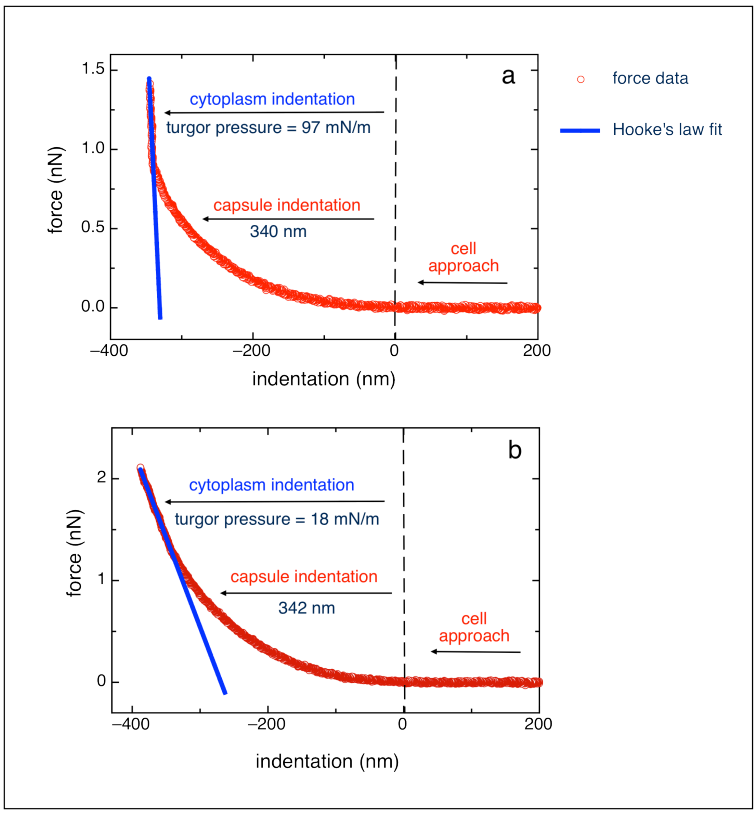

Figure 2. Typical force profiles (blue) of a *K. pneumoniae* cell with Hooke's law fit (red) in a) HEPES buffer, and b) 6 μM caerin solution. Derived parameters (capsule thickness and turgor pressure) shown.

Figure 2a shows a typical force profile for the indentation of a *K. pneumoniae* cell in buffer. In Figure 2b, the force profile shown is typical of lysed cells in 6 μM caerin solution. Hooke's law fit (Eq. 1) has been applied to the linear portion of both curves. It is this stage of cell indentation that corresponds to the point where the loading force on the cell is of sufficient magnitude that the dominant opposing force is the turgor pressure of the cell. The gradient of the linear Hooke's law fit is the turgor pressure of the cell. The turgor pressure of a bacterial cell is a measure of the osmotic stability and viability of the cell.

Figure 3 contains plots of turgor pressure and capsule thickness for three of the 10 single cell experiments in this study. The three cells depicted here were chosen because their turgor

pressure plots are representative of a type of behaviour observed when exposed to caerin. In Figure 3a, a large increase in turgor pressure to ~250 mN/m, indicative of increased osmotic stress, is seen in the first 90 minutes, significantly greater than the average turgor pressure of cells in buffer (118 ± 40 mN/m) and indicative of increased osmotic pressure. Measurements then plateaued for the remaining period of observation. Four of 10 single cells showed this behaviour. In Figure 3c, the cell underwent a very large turgor pressure increase to 784 mN/m followed by a rapid decrease. Two of 10 single cells showed this behaviour. Turgor pressure reduction after reaching a maximum is suggestive of lysis and cytoplasm leakage from a compromised envelope/membrane. This observation is in good agreement with previous work. [35, 55] Figure 3e shows a steady turgor pressure reduction until measurements plateaued at a value typical of lysed cells (~15 mN/m) [56]. Four of 10 single cells showed this behaviour.

These three behaviours can be considered as part of the same process: the increased osmotic pressure that occurs due to the accumulation of peptide at the outer membrane followed by lysis and turgor pressure reduction. We speculate that the cells that behave like those in Figure 3a may withstand caerin exposure and the cells in Figure 3e may have experienced increased osmotic pressure prior to lysis. Turgor pressure changes in the data presented here indicate that peptide accumulation at the membrane has taken place. If peptide were accumulating within the capsule or interacting with lipopolysaccharide molecules, there would be no change in the linear region of force curves that report on turgor pressure. The variation in the kinetics of turgor pressure loss reported here has been observed in previous work [35] and is an expectation when performing quantitative measurements of biological systems as large natural variation exists within populations. [42, 57]

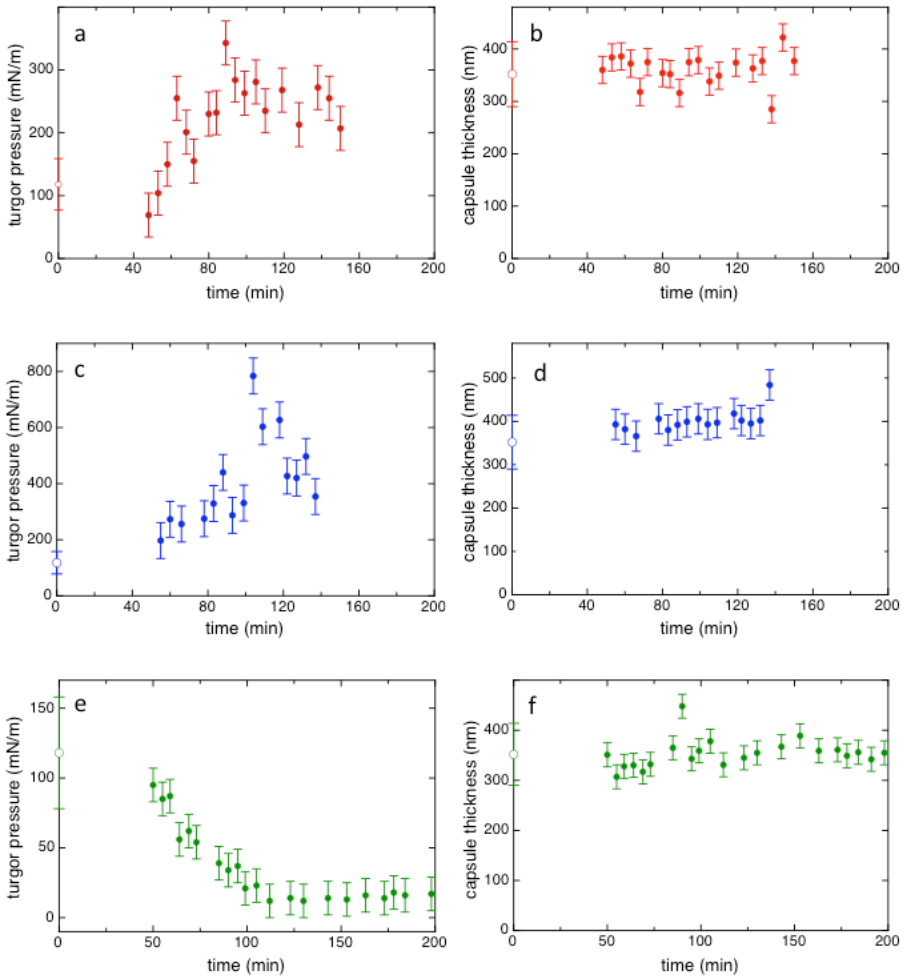

Figure 3. Turgor pressure and capsule thickness data for three representative *K. pneumoniae* cells submerged in 6 μM caerin solution.

Figures 3b, 3d and 3f show the capsule thickness measurements for the three representative cells. As in our previous work with a melittin analogue, capsule thickness measurements did not change appreciably. A change in capsule thickness was evident only at long exposure times (as in Fig. 3b & 3d at ~130 min) or at times associated with lysis (as in Fig. 3f at 85 min). This was also in good agreement with our previous work with melittin, although initially surprising since a cationic peptide would be expected to interact electrostatically with an anionic polysaccharide capsule. [58] Ionic interation would reduce polysaccharide

segment-segment repulsion and a collapse of the capsule and its brush-like structure (shown to exist in the *K. pneumoniae* capsule, [31]) would be expected. Such changes were not seen for either peptide. The changes in turgor pressure observed throughout the experiments reported here suggest that the peptide rapidly translocates through the capsule without any long-lived electrostatic association. Long-range electrostatic attraction may play a role in peptide-cell interactions but these results suggest that it is the entropic drive of the peptide to associate with the bacterial membrane that dominates. As was the case with melittin, similar MICs of 125 μM were obtained for both the wild-type and the capsule-deficient mutant, further evidence that the capsule confers no advantage to caerin exposure. To further understand the kinetics of peptide action, viable count assays of *K. pneumoniae* wild-type and capsule-deficient cells exposed to 6 μM caerin and melittin solutions were performed (Supporting information, Figure S2). The exposure of *K. pneumoniae* wild-type and capsule-deficient cells to 6 μM caerin resulted in a reduction of viable cell number of ~4.5 x 10^6 cfu/ml to ~2.0 x 10^4 cfu/ml within the first hour, corresponding to a 95% reduction, after which cell numbers remained constant after 24 hours. Melittin was found to be more bacteriostatic than caerin, where after a one-hour exposure time, no viable wild-type nor capsule-deficient cells were observed. These results are consistent with MIC/MBC data demonstrating that the MIC of caerin is three times larger than that of melittin, and no difference in susceptibility to either peptide was observed between wild-type and capsule-deficient cells (Supporting information, Figure S2).

Uniquely for caerin was the formation of 'holes' in the bacterial surface during the time course of an experiment as shown in Figure 4. The cell, shown in both height and deflection images, corresponds to the turgor pressure and capsule thickness data shown in green in Figure 3e and 3f. The cell was chosen for measurement due to its regular shape, average size

and adherence to the gelatine coated slides after initial scanning. It was first imaged at 50 minutes exposure time. At 85 minutes, the tip registered some interference, manifest in the 'lines' visible across both the height and deflection images (Fig. 4c & 4d). This corresponds to the high capsule thickness measurement at 85 minutes in Figure 3f. Tip interference of this type was evident in all the subsequent images. One hole first became apparent at 95 minutes exposure time, but the interference with the tip blurred the image and those that followed. By 120 minutes, imaging with less tip interference was possible (Fig. 4e & 4f) and several small and one large hole were visible. The holes were observed to grow to the size shown in Figures 4g and 4h at 173 minutes exposure time. The cell was observed for a further 25 minutes with no significant change.

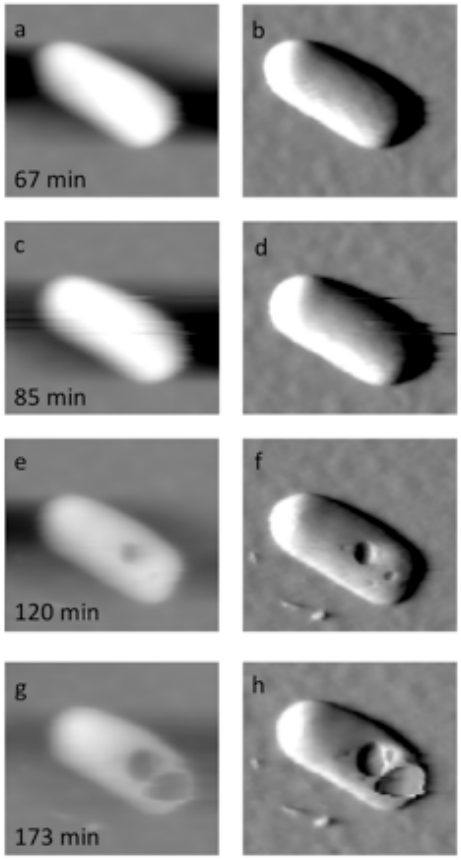

Figure 4. Height and deflection images (3 × 3.4 μm) of *K. pneumoniae* cells submerged in 6 μM caerin solution at a) and b) 67 minutes; c) and d) 85 minutes; e) and f) 120 minutes; and g) and h) 173 minutes exposure time.

Several cells that had not been subjected to successive force curve collection and imaging cycles also had similar damage, confirming that this phenomenon was not a product of AFM measurements. Damage of this kind, originating from very small defects, points to localised damage in the cell wall induced by caerin. A similar phenomenon was observed using AFM time lapse imaging by Rakowska *et al*. [59] in supported lipid bilayers exposed to a *de novo* peptide generated as an ideal model of a transmembrane AMP. As in our experiments with *K. pneumoniae*, the pores formed in the supported lipid bilayer experiments of Rakowska *et al*. were not limited to a particular size but could expand laterally on both the nano-to-micrometer scale. To observe the effect of caerin exposure on the cytoplasmic and outer membranes, cells treated with caerin were visualised using cryo-electron microscopy.

Figure 5a shows a single *K. pneumoniae* cell treated with buffer only. Cytoplasmic membrane, peptidoglycan layer, outer membrane and fimbriae are all clearly visible. Figure 5 b and 5c show cells treated with caerin for two hours before flash freezing for cryo-EM. Two different caerin concentrations were used. Firstly, the concentration at which AFM measurements were taken, 6 μM (Fig. 5b), and a higher concentration, three times the MIC, at 380 μM (Fig. 5c) to ensure cells were captured in a damaged state, as caerin did not lyse cells in four out of 10 AFM single cell experiments.

Sixty cells were visualised at 6 μM. Of these, five cells showed damage of the kind in Figure 5b where cytoplasmic membrane is no longer visible and peptidoglycan only partially evident. A further 20 cells showed membrane or peptidoglycan discontinuities and the remaining 35 cells showed no visible damage. This is in good agreement with AFM data that showed cells were not uniformly affected by caerin.

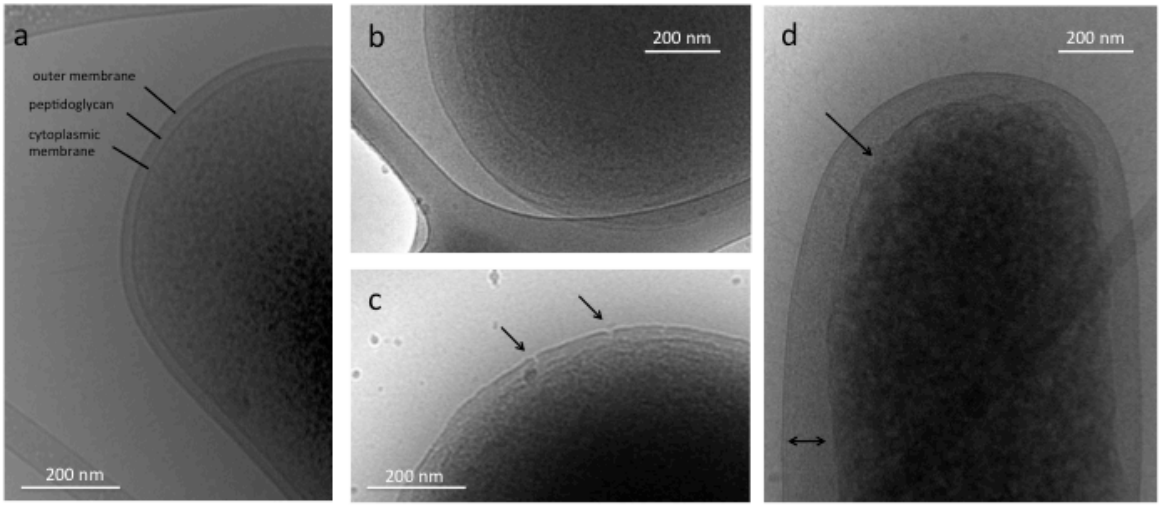

Figure 5: Cryo-electron micrographs of *K. pneumoniae* cells treated with: a) HEPES buffer; b) in 6 μM caerin; c) 380 μM caerin, arrows indicate the presence of 'holes' or 'cracks' in the outer membrane; and d) 6 μM melittin. Swelling of periplasm indicated by doubled-headed arrow, cytoplasmic membrane discontinuity indicated by arrow.

Cryo-EM images of melittin-treated cells (6 μM) showed a higher proportion of cells (14 of 18) visualised with swelling of the periplasm as in Figure 5d, reflecting the lower MIC (38 μM [35]). The outer membrane and peptidoglycan layer appear to be intact. The cytoplasmic membrane appears to be sufficiently intact to contain the cellular contents, though it appears irregular and discontinuous in places. This contrasts with caerin-treated cells, where cellular contents appeared to be no longer contained. The distance between outer membrane and peptidoglycan layer and the cytoplasmic membrane is greater in treated cells, most probably reflecting a state of post-osmotic stress-induced lysis. A similar phenomenon was observed previously with *K. pneumoniae* and the antibiotic cyclic lipopeptide colistin [56]. Of the four remaining melittin-treated cells, three had discontinuous cytoplasmic membranes and one cell appeared to be free of damage.

At 380 μM caerin, 27 of 37 cells visualised had no distinct cytoplasmic membrane and only partially visible peptidoglycan layers. Of these, 19 cells showed 'cracks' or 'holes' (~20 nm) in the outer membrane as marked with arrows in Figure 5c. A further 9 cells showed membrane discontinuities and one remaining cell showed no visible damage. The AFM images in Figure 4 show that the large 'holes' arise from very small defects. It is unclear though if these 'cracks', visible by cryo-EM at a high concentrations of caerin, are related to these small defects.

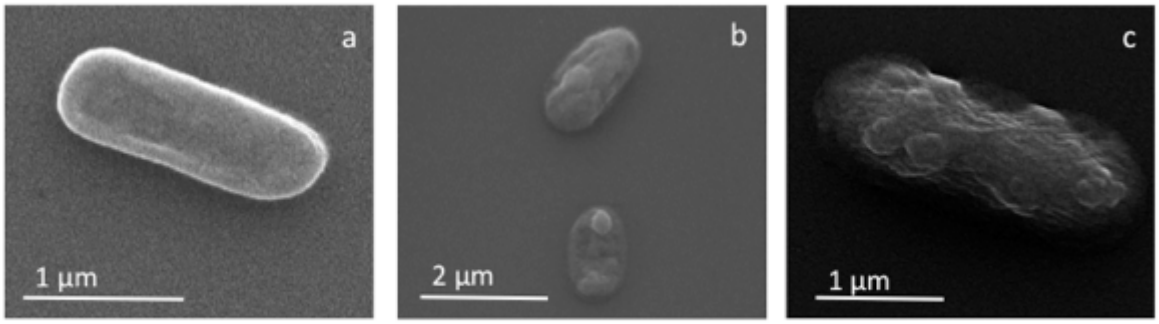

Figure 6: Scanning electron microscopy (SEM) images of *K. pneumoniae* treated with a) HEPES buffer; b) 6 μM caerin solution; and c) 380 μM caerin solution.

Scanning electron microscopy was used to further examine the cells. A cell treated with buffer (Fig. 6a) shows evidence of the dehydrating preparation. In Figure 6b, two cells treated with 6 μM caerin are shown. As in AFM and cryo-EM experiments, SEM images of caerin-treated cells do not indicate a uniform affect. Of the 38 cells visualised at this concentration, 14 displayed the kind of damage visible in the lower of the two cells. The remaining 24 cells showed damage that could not be easily distinguished from the effect of dehydration on the cells (as shown in the upper of the two cells). At 380 μM, 26 cells were visualised. Of these, 20 cells were severely damaged as in Figure 6c. The remaining 6 cells showed damage that could not be easily distinguished from the effect of dehydration on the cells. The caerin-

damaged cells in Figure 6b and 6c show cells with concave damage, in good agreement with the 'holes' found in AFM experiments.

Conclusions

Time-resolved AFM images revealed caerin caused localized defects in the cell wall of lysed *K. pneumoniae*, pointing to a pore-forming mechanism of action. These defects continued to grow to become large holes that were also visualised by scanning electron microscopy. Evidence of damaged membranes was visualised by cryo-EM at the concentration used in AFM experiments. At three times the MIC, 'pores' in the outer membrane were visible. In addition, the *K. pneumoniae* AJ218 capsule was largely unchanged by exposure to caerin, indicating that ionic interaction with bacteria-bound capsular polysaccharide was not a key factor for AMP interaction with *K. pneumoniae* AJ218 cells. Further, the presence of a capsule conferred no resistance advantage to wild-type over capsule-deficient cells when exposed to caerin. Caerin 1.1 appears to affect the mechanobiology of bacteria via membrane pore formation.

Acknowledgements

The authors gratefully acknowledge Michelle Gee for her support, the support of the Australian Research Council and the National Health and Medical Research Council (Program Grant 606788). AM received an Australian Postgraduate Award. AFM work was performed in part at the Materials Characterization and Fabrication Platform (MCFP) at the University of Melbourne.

Supporting Information Available

Figure S1: Reproducibility of force curves

Figure S2: Viable count assay

References

[1] P. Andreas, S. Hans-Georg, The co-evolution of host cationic antimicrobial peptides and microbial resistance, Nat. Rev. Microbiol., 4 (2006) 529-536.
[2] M.R. Yeaman, A.S. Bayer, Antimicrobial Peptides Versus Invasive Infections, in: W. Shafer (Ed.) Antimicrobial Peptides and Human Disease, vol. 306, Springer Berlin Heidelberg, 2006, pp. 111-152.
[3] R.M. Epand, R.F. Epand, Bacterial membrane lipids in the action of antimicrobial agents, J. Pept. Sci., 17 (2011) 298-305.
[4] R.E.W. Hancock, Peptide antibiotics, Lancet, 349 (1997) 418.
[5] Y. Shai, Mode of action of membrane active antimicrobial peptides, Peptide Science, 66 (2002) 236-248.
[6] S. Joshi, G.S. Bisht, D.S. Rawat, A. Kumar, R. Kumar, S. Maiti, S. Pasha, Interaction studies of novel cell selective antimicrobial peptides with model membranes and E. coli ATCC 11775, BBA-Biomembranes, 1798 (2010) 1864-1875.
[7] A. Tossi, L. Sandri, A. Giangaspero, Amphipathic, α-helical antimicrobial peptides, Peptide Science, 55 (2000) 4-30.
[8] Y. Shai, Mechanism of the binding, insertion and destabilization of phospholipid bilayer membranes by α-helical antimicrobial and cell non-selective membrane-lytic peptides, BBA-Biomembranes, 1462 (1999) 55-70.
[9] E. Strandberg, J. Zerweck, P. Wadhwani, Anne S. Ulrich, Synergistic Insertion of Antimicrobial Magainin-Family Peptides in Membranes Depends on the Lipid Spontaneous Curvature, Biophys. J., 104 (2013) L9-L11.
[10] R. Chen, A. Mark, The effect of membrane curvature on the conformation of antimicrobial peptides: implications for binding and the mechanism of action, Eur Biophys J, 40 (2011) 545-553.
[11] D.I. Fernandez, J.D. Gehman, F. Separovic, Membrane interactions of antimicrobial peptides from Australian frogs, BBA-Biomembranes, 1788 (2009) 1630-1638.
[12] M. Dathe, T. Wieprecht, Structural features of helical antimicrobial peptides: their potential to modulate activity on model membranes and biological cells, BBA-Biomembranes, 1462 (1999) 71-87.
[13] N. Papo, Y. Shai, Can we predict biological activity of antimicrobial peptides from their interactions with model phospholipid membranes?, Peptides, 24 (2003) 1693-1703.
[14] M.L. Gee, M. Burton, A. Grevis-James, M.A. Hossain, S. McArthur, E.A. Palombo, J.D. Wade, A.H.A. Clayton, Imaging the action of antimicrobial peptides on living bacterial cells, Sci Rep, 3 (2013).
[15] R.F. Epand, R.I. Lehrer, A. Waring, W. Wang, R. Maget-Dana, D. Lelièvre, R.M. Epand, Direct comparison of membrane interactions of model peptides composed of only Leu and Lys residues, Peptide Science, 71 (2003) 2-16.

[16] D.I. Fernandez, M.-A. Sani, A.J. Miles, B.A. Wallace, F. Separovic, Membrane defects enhance the interaction of antimicrobial peptides, aurein 1.2 versus caerin 1.1, BBA-Biomembranes, 1828 (2013) 1863-1872.
[17] M.-A. Sani, S.T. Henriques, D. Weber, F. Separovic, Bacteria May Cope Differently from Similar Membrane Damage Caused by the Australian Tree Frog Antimicrobial Peptide Maculatin 1.1, Journal of Biological Chemistry, 290 (2015) 19853-19862.
[18] H. Wong, J.H. Bowie, J.A. Carver, The solution structure and activity of caerin 1.1, an antimicrobial peptide from the Australian green tree frog, Litoria splendida, Eur. J. Biochem., 247 (1997) 545-557.
[19] M.P. Boland, F. Separovic, Membrane interactions of antimicrobial peptides from Australian tree frogs, BBA-Biomembranes, 1758 (2006) 1178-1183.
[20] M.A. Apponyi, T.L. Pukala, C.S. Brinkworth, V.M. Maselli, J.H. Bowie, M.J. Tyler, G.W. Booker, J.C. Wallace, J.A. Carver, F. Separovic, J. Doyle, L.E. Llewellyn, Host-defence peptides of Australian anurans: structure, mechanism of action and evolutionary significance, Peptides, 25 (2004) 1035-1054.
[21] S.E. VanCompernolle, R.J. Taylor, K. Oswald-Richter, J. Jiang, B.E. Youree, J.H. Bowie, M.J. Tyler, J.M. Conlon, D. Wade, C. Aiken, T.S. Dermody, V.N. KewalRamani, L.A. Rollins-Smith, D. Unutmaz, Antimicrobial Peptides from Amphibian Skin Potently Inhibit Human Immunodeficiency Virus Infection and Transfer of Virus from Dendritic Cells to T Cells, Journal of Virology, 79 (2005) 11598-11606.
[22] G. McCubbin, S. Praporski, S. Piantavigna, D. Knappe, R. Hoffmann, J. Bowie, F. Separovic, L. Martin, QCM-D fingerprinting of membrane-active peptides, Eur Biophys J, 40 (2011) 437-446.
[23] C.S. Brian Chia, Y. Gong, J.H. Bowie, J. Zuegg, M.A. Cooper, Membrane binding and perturbation studies of the antimicrobial peptides caerin, citropin, and maculatin, Peptide Science, 96 (2011) 147-157.
[24] H.-J.r. Butt, B. Cappella, M. Kappl, Force measurements with the atomic force microscope: Technique, interpretation and applications, Surf. Sci. Rep., 59 (2005) 1-152.
[25] M. Radmacher, Measuring the elastic properties of biological samples with the AFM, Engineering in Medicine and Biology Magazine, IEEE, 16 (1997) 47-57.
[26] S.K. Lower, M.F. Hochella, T.J. Beveridge, Bacterial Recognition of Mineral Surfaces: Nanoscale Interactions Between Shewanella and α-FeOOH, Science, 292 (2001) 1360-1363.
[27] V. Dupres, F.D. Menozzi, C. Locht, B.H. Clare, N.L. Abbott, S. Cuenot, C. Bompard, D. Raze, Y.F. Dufrêne, Nanoscale mapping and functional analysis of individual adhesins on living bacteria, Nature Methods, 2 (2005) 515-520.
[28] P. Polyakov, C. Soussen, J. Duan, J.F.L. Duval, D. Brie, G. Francius, Automated Force Volume Image Processing for Biological Samples, PLoS ONE, 6 (2011) 1-19.
[29] G. Francius, P. Polyakov, J. Merlin, Y. Abe, J.-M. Ghigo, C. Merlin, C. Beloin, J.F.L. Duval, Bacterial Surface Appendages Strongly Impact Nanomechanical and Electrokinetic Properties of <italic>Escherichia coli</italic> Cells Subjected to Osmotic Stress, PLoS ONE, 6 (2011) e20066.
[30] H. Wang, J.J. Wilksch, T. Lithgow, R.A. Strugnell, M.L. Gee, Nanomechanics measurements of live bacteria reveal a mechanism for bacterial cell protection: the polysaccharide capsule in Klebsiella is a responsive polymer hydrogel that adapts to osmotic stress, Soft Matter, 9 (2013) 7560-7567.
[31] F. Gaboriaud, M.L. Gee, R. Strugnell, J.F.L. Duval, Coupled Electrostatic, Hydrodynamic, and Mechanical Properties of Bacterial Interfaces in Aqueous Media, Langmuir, 24 (2008) 10988-10995.

[32] J.E. Shaw, R.F. Epand, J.C.Y. Hsu, G.C.H. Mo, R.M. Epand, C.M. Yip, Cationic peptide-induced remodelling of model membranes: Direct visualization by in situ atomic force microscopy, Journal of Structural Biology, 162 (2008) 121-138.
[33] J. Strauss, A. Kadilak, C. Cronin, C.M. Mello, T.A. Camesano, Binding, inactivation, and adhesion forces between antimicrobial peptide cecropin P1 and pathogenic E. coli, Colloids Surf., B, 75 (2010) 156-164.
[34] F.-S. Kao, Y.-R. Pan, R.-Q. Hsu, H.-M. Chen, Efficacy verification and microscopic observations of an anticancer peptide, CB1a, on single lung cancer cell, BBA-Biomembranes, 1818 (2012) 2927-2935.
[35] A. Mularski, J.J. Wilksch, H. Wang, M.A. Hossain, J.D. Wade, F. Separovic, R.A. Strugnell, M.L. Gee, Atomic Force Microscopy Reveals the Mechanobiology of Lytic Peptide Action on Bacteria, Langmuir, (2015).
[36] M.A.T. Karthikeyan K Kumarasamy, Timothy R Walsh, Jay Bagaria, Fafhana Butt, Ravikumar Balakrishnan, Uma Chaudhary, Michel Doumith, Christian G Giske, Seema Irfan, Padma Krishnan, Anil V Kumar, Sunil Maharjan, Shazad Mushtaq, Tabassum Noorie, David L Paterson, Andrew Pearson, Claire Perry, Rachel Pike, Bhargavi Rao, Ujjwayini Ray, Jayanta B Sarma, Madhu Sharma, Elizabeth Sheridan, Mandayam A Thirunarayan, Jane Turton PhD, Supriya Upadhyay, Marina Warner, William Welfare, David M Livermore and Neil Woodford, Emergence of a new antibiotic resistance mechanism in India, Pakistan, and the UK: a molecular, biological, and epidemiological study, The Lancet Infectious Diseases, 10 (2010) 597-602.
[37] C.f.D.C.a. Prevention, Antibiotic Resistance Threats in the United States, 2013, in, 2013.
[38] S.P. Dzul, M.M. Thornton, D.N. Hohne, E.J. Stewart, A.A. Shah, D.M. Bortz, M.J. Solomon, J.G. Younger, Contribution of the Klebsiella pneumoniae Capsule to Bacterial Aggregate and Biofilm Microstructures, Appl. Environ. Microbiol., 77 (2011) 1777-1782.
[39] C. Struve, K.A. Krogfelt, Role of capsule in Klebsiella pneumoniae virulence: lack of correlation between in vitro and in vivo studies, FEMS Microbiol. Lett., 218 (2003) 149-154.
[40] M.A. Schembri, J. Blom, K.A. Krogfelt, P. Klemm, Capsule and Fimbria Interaction in Klebsiella pneumoniae, Infect. Immun., 73 (2005) 4626-4633.
[41] A.K. Highsmith, W.R. Jarvis, Klebsiella pneumoniae: Selected Virulence Factors That Contribute to Pathogenicity, Infection Control, 6 (1985) 75-77.
[42] E. Llobet, J.M. Tomas, J.A. Bengoechea, Capsule polysaccharide is a bacterial decoy for antimicrobial peptides, Microbiology, 154 (2008) 3877-3886.
[43] J.D. Gehman, F. Luc, K. Hall, T.-H. Lee, M.P. Boland, T.L. Pukala, J.H. Bowie, M.-I. Aguilar, F. Separovic, Effect of Antimicrobial Peptides from Australian Tree Frogs on Anionic Phospholipid Membranes†, Biochemistry, 47 (2008) 8557-8565.
[44] A.W. Jenney, A. Clements, J.L. Farn, O.L. Wijburg, A. McGlinchey, D.W. Spelman, T.L. Pitt, M.E. Kaufmann, L. Liolios, M.B. Moloney, S.L. Wesselingh, R.A. Strugnell, Seroepidemiology of Klebsiella pneumoniae in an Australian Tertiary Hospital and Its Implications for Vaccine Development, J. Clin. Microbiol., 44 (2006) 102-107.
[45] J. Yang, J.J. Wilksch, J.W.H. Tan, D.M. Hocking, C.T. Webb, T. Lithgow, R.M. Robins-Browne, R.A. Strugnell, Transcriptional Activation of the <italic>mrkA</italic> Promoter of the <italic>Klebsiella pneumoniae</italic> Type 3 Fimbrial Operon by the c-di-GMP-Dependent MrkH Protein, PLoS ONE, 8 (2013) e79038.
[46] V. de Lorenzo, M. Herrero, U. Jakubzik, K.N. Timmis, Mini-Tn5 transposon derivatives for insertion mutagenesis, promoter probing, and chromosomal insertion of cloned DNA in gram-negative eubacteria, J. Bacteriol., 172 (1990) 6568-6572.

[47] Y.M. Kwon, S.C. Ricke, Efficient amplification of multiple transposon-flanking sequences, Journal of Microbiological Methods, 41 (2000) 195-199.
[48] N.C.f.C.L. Standards, Methods for Dilution Antimicrobial Susceptibility Tests for Bacteria That Grow Aerobically, in, Pennsylvania, United States of America, 2003, pp. 14-17.
[49] J.L. Ingraham, O. Marloe, F.C. Neidhardt, Growth of the bacterial cell, Sinauer Associates, Sunderland, Mass., 1983.
[50] J.L. Hutter, J. Bechhoefer, Calibration of atomic‐force microscope tips, Rev. Sci. Instrum., 64 (1993) 1868-1873.
[51] S.B. Velegol, B.E. Logan, Contributions of Bacterial Surface Polymers, Electrostatics, and Cell Elasticity to the Shape of AFM Force Curves, Langmuir, 18 (2002) 5256-5262.
[52] M. Radmacher, M. Fritz, P.K. Hansma, Imaging soft samples with the atomic force microscope: gelatin in water and propanol, Biophys. J., 69 (1995) 264-270.
[53] F. Gaboriaud, B.S. Parcha, M.L. Gee, J.A. Holden, R.A. Strugnell, Spatially resolved force spectroscopy of bacterial surfaces using force-volume imaging, Colloids Surf., B, 62 (2008) 206-213.
[54] Z. Suo, R. Avci, M. Deliorman, X. Yang, D.W. Pascual, Bacteria Survive Multiple Puncturings of Their Cell Walls, Langmuir, 25 (2009) 4588-4594.
[55] S. Liu, A.K. Ng, R. Xu, J. Wei, C.M. Tan, Y. Yang, Y. Chen, Antibacterial action of dispersed single-walled carbon nanotubes on Escherichia coli and Bacillus subtilis investigated by atomic force microscopy, Nanoscale, 2 (2010) 2744-2750.
[56] A. Mularski, Wilksch, J. J., Hanssen, E., Li, J., Tomita, T., Pidot, S. J., Stinear, T., Gee, M., Separovic, F., Strugnell, D., A nanomechanical study of the effects of colistin on the Klebsiella pneumoniae AJ218 capsule, unpublished.
[57] M.G.J.L. Habets, D.E. Rozen, M.A. Brockhurst, Variation in Streptococcus pneumoniae susceptibility to human antimicrobial peptides may mediate intraspecific competition, Proc. R. Soc. London, B, (2012).
[58] G.G.S. Dutton, E.H. Merrifield, The capsular polysaccharide from Klebsiella serotype K54; location of the O-acyl groups, and a revised structure, Carbohydr. Res., 105 (1982) 189-203.
[59] P.D. Rakowska, H. Jiang, S. Ray, A. Pyne, B. Lamarre, M. Carr, P.J. Judge, J. Ravi, U.I. M. Gerling, B. Koksch, G.J. Martyna, B.W. Hoogenboom, A. Watts, J. Crain, C.R.M. Grovenor, M.G. Ryadnov, Nanoscale imaging reveals laterally expanding antimicrobial pores in lipid bilayers, Proc. Natl. Acad. Sci. U. S. A., 110 (2013) 8918-8923.

Author/s:
Mularski, A; Wilksch, JJ; Hanssen, E; Strugnell, RA; Separovic, F

Title:
Atomic force microscopy of bacteria reveals the mechanobiology of pore forming peptide action

Date:
2016-06-01

Citation:
Mularski, A., Wilksch, J. J., Hanssen, E., Strugnell, R. A. & Separovic, F. (2016). Atomic force microscopy of bacteria reveals the mechanobiology of pore forming peptide action. BIOCHIMICA ET BIOPHYSICA ACTA-BIOMEMBRANES, 1858 (6), pp.1091-1098. https://doi.org/10.1016/j.bbamem.2016.03.002.